Chinese Journal of Natural Medicines

Azaphilone derivatives with RANKL-induced osteoclastogenesis inhibition from the mangrove endophytic fungus *Diaporthe* sp.

Miaoping Lin, Yanhui Tan, Humu Lu, Yuyao Feng, Min Li, Chenghai Gao, Yonghong Liu, Xiaowei Luo

Citation: Miaoping Lin, Yanhui Tan, Humu Lu, Yuyao Feng, Min Li, Chenghai Gao, Yonghong Liu, Xiaowei Luo, Azaphilone derivatives with RANKL-induced osteoclastogenesis inhibition from the mangrove endophytic fungus *Diaporthe* sp., Chinese Journal of Natural Medicines, 2025, 23(9), 1143-1152. doi: 10.1016/S1875-5364(25)60974-5.

View online: https://doi.org/10.1016/S1875-5364(25)60974-5

Chinese Journal of Natural Medicines 23 (2025) 1143-1152

Contents lists available at ScienceDirect

Chinese Journal of Natural Medicines

journal homepage: www.cjnmcpu.com/

Original article

Azaphilone derivatives with RANKL-induced osteoclastogenesis inhibition from the mangrove endophytic fungus *Diaporthe* sp.

Miaoping Lin[a,c,Δ], Yanhui Tan[b,Δ], Humu Lu[a], Yuyao Feng[a], Min Li[b], Chenghai Gao[a], Yonghong Liu[a,*], Xiaowei Luo[a,*]

[a] *Guangxi Key Laboratory of Marine Drugs, University Engineering Research Center of High-efficient Utilization of Marine Traditional Chinese Medicine Resources, Guangxi, Institute of Marine Drugs, Guangxi University of Chinese Medicine, Nanning 530200, China*

[b] *State Key Laboratory for Chemistry and Molecular Engineering of Medicinal Resources, School of Chemistry and Pharmaceutical Sciences, Guangxi Normal University, Guilin 541004, China*

[c] *The First Affiliated Hospital of Guangxi University of Chinese Medicine, Nanning 530023, China*

ARTICLE INFO

Article history:
Received 3 July 2024
Revised 26 October 2024
Accepted 29 October 2024
Available online 20 September 2025

Keywords:
Marine fungus
Diaporthe sp.
Azaphilones
Anti-osteoclastogenesis

ABSTRACT

This study identified six novel azaphilones, isochromophilones G–L (**1**–**6**), and three novel biosynthetically related congeners (**7**–**9**) from *Diaporthe* sp. SCSIO 41011. The structures and absolute configurations were elucidated through comprehensive spectroscopic analyses combined with experimental and calculated electronic circular dichroism (ECD) spectra. Significantly, three highly oxygenated azaphilones contain an acetyl group at the terminal chain (**4**) or linear conjugated polyenoid moieties (**5** and **6**), which occur infrequently in the azaphilone family. Additionally, several compounds demonstrated inhibition of lipopolysaccharide (LPS)-induced nuclear factor kappa-B (NF-κB) activation in RAW 264.7 macrophages at 20 μmol·L^{-1}. The novel compound (**1**) effectively inhibited receptor activator of NF-κB ligand (RANKL)-induced osteoclast differentiation without exhibiting cytotoxicity in bone marrow and RAW 264.7 macrophages, indicating its potential as a promising lead compound for osteolytic disease treatment. This research presents the first documented evidence of azaphilone derivatives as inhibitors of RANKL-induced osteoclastogenesis.

1. Introduction

Osteoporosis is a metabolic bone disorder characterized by reduced bone mass and deterioration of bone tissue microarchitecture, leading to increased bone fragility and fracture risk [1–3]. This condition presents a significant public health challenge due to the aging population, particularly affecting postmenopausal women with estrogen deficiency [1]. The inhibition of osteoclast differentiation has emerged as an effective therapeutic approach for preventing excessive bone resorption, fractures, and pain in osteolytic diseases [4]. Osteoclasts are specialized multinucleated cells possessing bone-resorbing capabilities, formed through the fusion of committed monocyte/macrophage hematopoietic lineage precursor cells [5]. The receptor activator of nuclear factor kappa-B (NF-κB) ligand (RANKL) and macrophage colony-stimulating factor (M-CSF) are essential for osteoclast development and activation [6, 7]. Current first-line anti-osteoclast medications, denosumab and bisphosphate, present serious complications during long-term use, including jaw osteonecrosis, potentially leading to disability [2, 8]. Consequently, there is an urgent need for novel osteoclast differentiation inhibitors with alternative mechanisms of action for treating osteolytic diseases.

Marine microorganisms, particularly marine fungi, have recently emerged as significant underutilized sources of marine natural products [9]. Notably, mangrove-associated fungi, representing the second-largest ecological group of marine fungi, contribute substantially to their biosphere while producing structurally unique and diverse bioactive secondary metabolites [10, 11]. Marine microbial natural products have demonstrated potential as inhibitors of RANKL-induced osteoclastogenesis [12], including chlorinated depsides [13], phenols [14], sirenins [15], nitrobenzoyl sesquiterpenoids [4], and meroterpenoids [16]. Azaphilones, fungal pigments characterized by a highly oxygenated pyranoquinone bicyclic core [17], comprise over 700 compounds produced by 61 genera of filamentous fungi through the polyketide pathway [18]. These compounds have attracted attention from natural product chemists and pharmacologists due to their diverse structures and significant pharmacological properties [19]. Our previous research identified six new cytotoxic chloroazaphilones, isochromophilones A–F, from the mangrove-derived fungus *Diaporthe* sp. SCSIO 41011 [20]. Continuing our investigation of structurally diverse azaphilone analogues, we isolated four new sclerotiorin-type azaphilones (**1**–**4**), two new chrysodin-type (**5**–**6**) azaphilones, and three new congeners (**7**–**9**) from this strain, which was cultured on wheat solid medium using the "One Strain, Many Compounds" (OSMAC) strategy. Several compounds demonstrated suppression of RANKL-induced osteoclastogenesis, suggesting potential

* Corresponding author.
E-mail addresses: yonghongliu@scsio.ac.cn (Y. Liu); luoxiaowei1991@126.com (X. Luo)
Δ These authors contributed equally to this work.

https://doi.org/10.1016/S1875-5364(25)60974-5

lead compounds for osteolytic disease treatment. This paper describes the isolation, structural elucidation, and anti-osteoclastogenic activities of these azaphilones and their congeners.

2. Results and discussion

The EtOAc extract of *Diaporthe* sp. SCSIO 41011 from wheat solid fermentation underwent silica gel and semipreparative high performance liquid chromatography (HPLC) chromatography, yielding six new azaphilone derivatives (**1**–**6**), three new congeners (**7**–**9**), and two known compounds, trichopyrone C (**10**) [21] and *E*-7,9-diene-11-methenyl palmitic acid (**11**) [22] (Fig. 1).

Compound **1** was isolated as a yellow oil with the molecular formula $C_{22}H_{27}BrO_4$ (9 degrees of unsaturation, DOU) based on a cluster of deprotonated ion peaks at *m/z* 435.1177/437.1154 ($[M + H]^+$) with a ratio of 1∶1 in the high-resolution electrospray ionization mass spectrometry (HR-ESI-MS), indicating the presence of a bromide atom. Analysis of the ^{1}H nuclear magnetic resonance (NMR) (Table 1) and heteronuclear single quantum correlation (HSQC) data of **1** revealed resonances for five olefinic protons, H-1 (δ_H 6.88, s), H-4 (δ_H 6.58, s), H-9 (δ_H 6.08, d, *J* = 15.4 Hz), H-10 (δ_H 7.02, d, *J* = 15.4 Hz), and H-12 (δ_H 5.64, d, *J* = 9.8 Hz), two methines, H-8 (δ_H 3.35, dd, *J* = 9.8, 2.1 Hz) and H-13 (δ_H 2.48, m), two methylenes, H_2-14 (δ_H 1.43, m; 1.28, m), and H_2-1′ (δ_H 3.24, dd, *J* =16.8, 2.1 Hz; 2.75, dd, *J* =16.8, 9.8 Hz), and five methyls, including three singlet ones H_3-17 (δ_H 1.83), H_3-18 (δ_H 1.10) and H_3-3′ (δ_H 2.28), one doublet H_3-16 (δ_H 1.01, d, *J* = 6.3 Hz), and one terminal H_3-15 (δ_H 0.86, t, *J* = 7.0 Hz).

In addition to the 14 corresponding hydrogen-bearing carbons, eight carbons were identified in the ^{13}C NMR data (Table 2), comprising two carbonyls, five olefinics (one oxygenated), and one oxygenated tertiary carbon. The observed NMR characteristics demonstrated strong similarity to those of the previously co-isolated *epi*-isochromophilone II [20], with the notable distinction being the presence of a bromide atom at C-5 in **1** rather than a chlorine atom in *epi*-isochromophilone II. This structural difference was confirmed by the shielding effect on C-5 (δ_C 99.7 for **1**, 109.4 for *epi*-isochromophilone II) and the molecular formula. Additionally, this variation could be attributed to NaBr-induced fermentations based on the OSMAC approach. Analysis of 2D NMR correlations (Fig. 2) confirmed the planar structure of **1**, which was designated as isochromophilone G.

The coupling constant of $J_{H\text{-}9/H\text{-}10}$ = 15.4 Hz and the diagnostic nuclear Overhauser effect spectroscopy (NOESY) correlations (Fig. 3) between H-9/H_3-17 and H-10/H-12 demonstrated that both Δ^9 and Δ^{11} double bonds possessed the *E* configuration. Additionally, the NOESY correlation of H_3-18 (δ_H 1.10)/H_2-1′ (δ_H 3.24, 2.75) indicated that CH_3-18 and CH_2-1′ groups were positioned on the same face. The chiral center of C-13 in the aliphatic side chain was assigned the *S*-configuration, consistent with other sclerotiorin-type azaphilones from a biogenetic perspective [19, 20]. Given the unsuccessful crystallization attempts of azaphilones, quantum chemical electronic circular dichroism (ECD) calculation has proven to be a reliable and effective method for determining their absolute configurations [20, 23]. Consequently, two possible diastereoisomers of **1** underwent ECD calculations at B3LYP/6-31 + G (d, p) level using time-dependent density functional theory (TDDFT) [20]. The calculated ECD curve (Fig. 4) of (7*R*,8*S*,13*S*)-**1** aligned well with the experimental data, confirming the (7*R*,8*S*,13*S*)-configuration of **1**.

HR-ESI-MS analysis of isochromophilone H (**2**) yielded the molecular formula $C_{19}H_{26}O_4$ (7 DOUs). The ^{1}H NMR data (Table 1) of **2** revealed signals corresponding to four olefinic protons, H-4 (δ_H 5.40, s), H-9 (δ_H 5.91, d, *J* = 15.4 Hz), H-10 (δ_H 6.96, d, *J* = 15.4 H), and H-12 (δ_H 5.60, d, *J* = 9.8 Hz), two methines, H-6 (δ_H 4.04, dd, *J* = 10.0, 5.6 Hz) and H-13 (δ_H 2.43, m), three methylenes, H_2-1 (δ_H 5.01, d, *J* = 12.6 Hz; 4.83, d, *J* = 12.6 Hz), H_2-5 (δ_H 2.69, dd, *J* = 17.5, 5.6 Hz; 2.50, dd, *J* = 17.5, 10.0 Hz), and H_2-14 (δ_H 1.29–1.41, m), and five methyls, comprising two singlet ones H_3-17 (δ_H 1.79) and H_3-18 (δ_H 1.26), one doublet H_3-16 (δ_H 0.98, d, *J* = 6.3 Hz), and one terminal H_3-15 (δ_H 0.85, t, *J* = 7.7 Hz).

In addition, the ^{13}C NMR spectrum revealed 6 nonprotonated carbons, including one carbonyl (δ_C 196.8), four olefinics (δ_C 150.5, 132.2, 113.4, and an oxygenated one 161.9), and one oxygenated quaternary carbon (δ_C 77.3). The spectroscopic characteristics of **2** indicated an azaphilone-like structure, showing significant similarity to a key intermediate, (7*S*)-3-((*S*,1*E*,3*E*)-3,5-dimethylhepta-1,3-dien-1-yl)-6,7-dihydroxy-7-methyl-1,5,6,7-tetrahydro-8*H*-isochromen-8-one, produced through heterologous expression in *Aspergillus nidulans* [24]. Analysis of 2D NMR correlations of **2** indicated that both compounds shared identical planar structures.

As observed in **1**, the Δ^9 and Δ^{11} double bonds exhibited *E* configuration, confirmed by the large coupling constant of

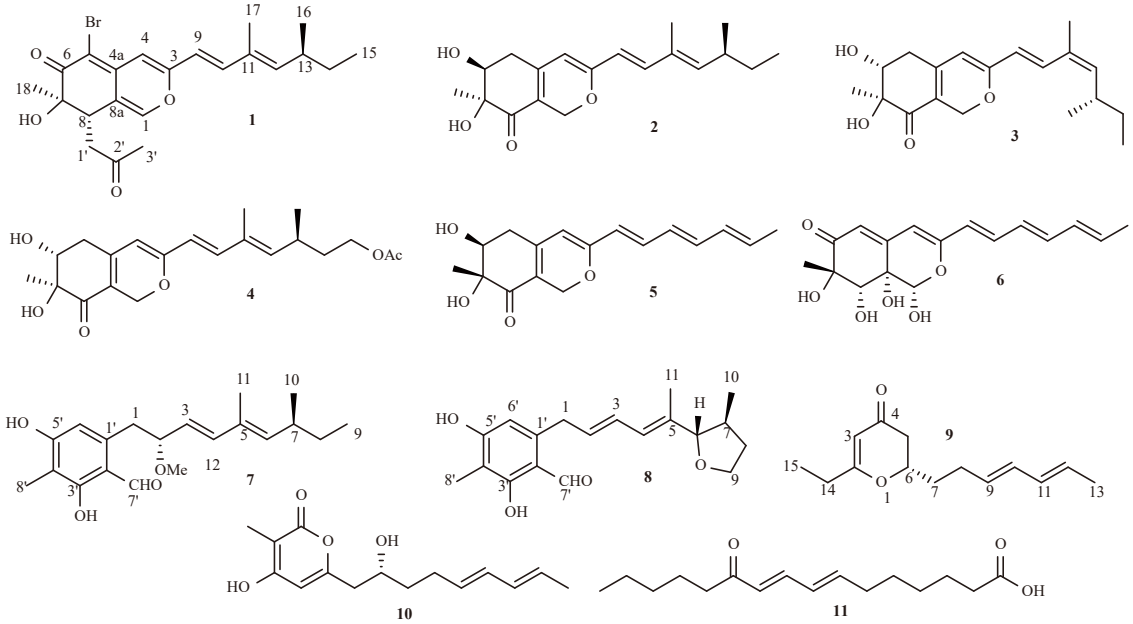

Fig. 1 Chemical structures of **1**–**11**.

Table 1 ^{1}H NMR (700 MHz) data for compounds **1**–**6** (*J* in Hz).

No.	**1**[a]	**2**[a]	**3**[a]	**4**[b]	**5**[a]	**6**[c]
1	6.88, s	5.01, d (12.6)	5.03, d (12.6)	4.88, d (12.6)	5.00, d (12.6)	5.40, s
		4.83, d (12.6)	4.86, d (12.6)	4.79, d (12.6)	4.83, d (12.6)	
4	6.58, s	5.40, s	5.43, s	5.60, s	5.38, s	5.77, s
5*α*		2.69, dd	2.49, dd	2.45, dd	2.68, dd	5.71, s
		(17.5, 5.6)	(17.5, 10.0)	(17.5, 5.6)	(17.5, 5.6)	
5*β*		2.50, dd	2.69, dd	2.68, dd	2.49, dd	
		(17.5, 10.0)	(17.5, 5.6)	(17.5, 10.0)	(17.5, 10.0)	
6		4.04, dd	4.04, dd	3.93, overlapped	4.03, dd	
		(10.0, 5.6)	(10.0, 5.6)		(10.0, 5.6)	
8	3.35, dd (9.8, 2.1)					3.97, s
9	6.08, d (15.4)	5.91, d (15.4)	6.00, d (15.4)	6.13, d (15.4)	5.95, d (15.4)	6.09, d (15.4)
10	7.02, d (15.4)	6.96, d (15.4)	7.32, d (15.4)	6.89, d (15.4)	6.92, dd	6.98, dd
					(15.4, 11.2)	(15.4, 11.2)
11					6.20, dd	6.27, dd
					(15.4, 11.2)	(15.4, 11.2)
12	5.64, d (9.8)	5.60, d (9.8)	5.42, d (7.0)	5.62, d (9.8)	6.44, dd	6.46, dd
					(15.4, 11.2)	(15.4, 11.2)
13	2.48, m	2.43, m	2.64, m	2.75, m	6.15, m	6.19, m
14	1.43, m	1.42, m	1.40, m	1.74, m	5.90, m	5.89, m
	1.28, m	1.29, m	1.26, m	1.59, m		
15	0.86, t (7.7)	0.85, t (7.7)	0.85, t (7.7)	3.93–4.04, m	1.83, d (7.0)	1.81, d (7.0)
16	1.01, d (6.3)	0.98, d (6.3)	0.98, d (6.3)	1.03, d (6.3)		
17	1.83, s	1.79, s	1.86, s	1.82, s		
18	1.10, s	1.27, s	1.26, s	1.19, s	1.26, s	1.38, s
1′	3.24, dd					
	(16.8, 2.1)					
	2.75, dd					
	(16.8, 9.8)					
2′				1.97, s		
3′	2.28, s					

[a]In $CDCl_3$; [b] In acetone-d_6; [c] In CD_3OD.

$J_{H\text{-}9/H\text{-}10}$ = 15.4 Hz and the NOESY correlations of H-9/H_3-17 and H-10/H-12. Additionally, the NOESY correlation of H-6 (δ_H 4.04)/H-5*α* (δ_H 2.69), H_3-18 (δ_H 1.27) demonstrated that H-6 and H_3-18 were positioned on the same face in the cyclohexanone unit. Furthermore, the calculated ECD spectra (Fig. 4) of **2** confirmed the (6*S*,7*S*,13*S*)-configuration.

Isochromophilone I (**3**) exhibited nearly identical spectroscopic characteristics to **2**, with notable differences in the chemical shifts of C-10 [δ_C 141.6 (**2**), 133.1 (**3**)], C-17 [δ_C 12.5 (**2**), 20.3 (**3**)], and H-10 [δ_H 6.96 (**2**), 7.32 (**3**)]. Analysis of 2D NMR correlations indicated that they were *E*- (**2**) and *Z*- (**3**) isomers of the Δ^{11} double bond, with **3** confirmed as *Z*-configuration through NOESY correlations of H-12/H_3-17 and H-10/H-13. The NOESY correlations of H-5*α* (δ_H 2.49)/H_3-18 (δ_H 1.26) and H-5*β* (δ_H 2.69)/H-6 (δ_H 4.04) indicated that H-6 and H_3-18 were positioned on opposite faces of the cyclohexanone unit. Comparison between experimental and calculated ECD spectra of **3** established the (6*R*,7*S*,13*S*)-configuration.

Isochromophilone J (**4**) was isolated as a yellow oil with a molecular formula of $C_{21}H_{28}O_6$ (8 DOUs), determined by HR-ESI-MS data, showing 58 mass units higher than **2**, corresponding to an $OCOCH_2$ group. The NMR spectral data of **4** exhibited close similarity to **2**, with the primary difference being an additional acetoxyl group [δ_C 170.9 (C-1′), 20.8 (C-2′); δ_H 1.97 (H_3-2′)] at C-15 in **4**, confirmed by the heteronuclear multiple bond correlation (HMBC) of H_2-15 (δ_H 3.93, m; 4.02, m)/C-1′ and H_3-2′/C-1′. The *E*-configuration of both Δ^9 and Δ^{11} double bonds and the opposite orientation of H-6 and H_3-18 in the cyclohexanone unit were determined through analysis of NOESY correlations (Fig. 3) and coupling constants of **4**. The Boltzmann-weighted ECD spectra of **4** were calculated using acetoxyl-removed structural models (Supplementary data, **Fig. S1**). The calculated ECD spectra

Table 2 ^{13}C NMR (175 MHz) data for **1**–**6**.

No.	**1**[a], type	**2**[a], type	**3**[a], type	**4**[b], type	**5**[a], type	**6**[c], type
1	143.7, CH	64.2, CH_2	64.2, CH_2	64.6, CH_2	64.2, CH_2	97.6, CH
3	158.5, C	161.9, C	161.7, C	161.0, C	161.2, C	159.6, C
4	107.7, CH	104.8, CH	105.5, CH	106.3, CH	105.4, CH	106.0, CH
4a	145.9, C	150.5, C	150.4, C	150.0, C	150.2, C	153.6, C
5	99.9, C	33.8, CH_2	33.8, CH_2	34.9, CH_2	33.8, CH_2	117.6, CH
6	192.5, C	73.1, CH	73.0, CH	73.4, CH	73.0, CH	199.0, C
7	74.1, C	77.3, C	77.3, C	77.6, C	77.3, C	76.4, C
8	40.5, CH	196.8, C	196.9, C	197.9, C	196.8, C	74.8, CH
8a	120.3, C	113.4, C	113.7, C	115.1, C	113.8, C	71.2, C
9	116.5, CH	118.1, CH	120.5, CH	120.1, CH	123.0, CH	125.4, CH
10	142.2, CH	141.6, CH	133.1, CH	140.2, CH	136.6, CH	136.5, CH
11	132.1, C	132.2, C	130.3, C	133.7, C	129.1, CH	130.6, CH
12	147.9, CH	146.9, CH	144.5, CH	144.6, CH	139.0, CH	139.1, CH
13	35.2, CH	35.1, CH	34.0, CH	30.7, CH	131.7, CH	133.1, CH
14	30.2, CH_2	30.3, CH_2	30.4, CH_2	36.6, CH_2	134.2, CH	133.8, CH
15	12.1, CH_3	12.1, CH_3	12.1, CH_3	63.1, CH_2	18.8, CH_3	18.6, CH_3
16	20.4, CH_3	20.5, CH_3	21.1, CH_3	20.9, CH_3		
17	12.5, CH_3	12.5, CH_3	20.3, CH_3	12.4, CH_3		
18	21.4, CH_3	18.4, CH_3	18.3, CH_3	18.6, CH_3	18.3, CH_3	20.8, CH_3
1′	40.0, CH_2			170.9, C		
2′	207.1, C			20.8, CH_3		
3′	30.0, CH_3					

[a] In $CDCl_3$; [b] In acetone-d_6; [c] In CD_3OD.

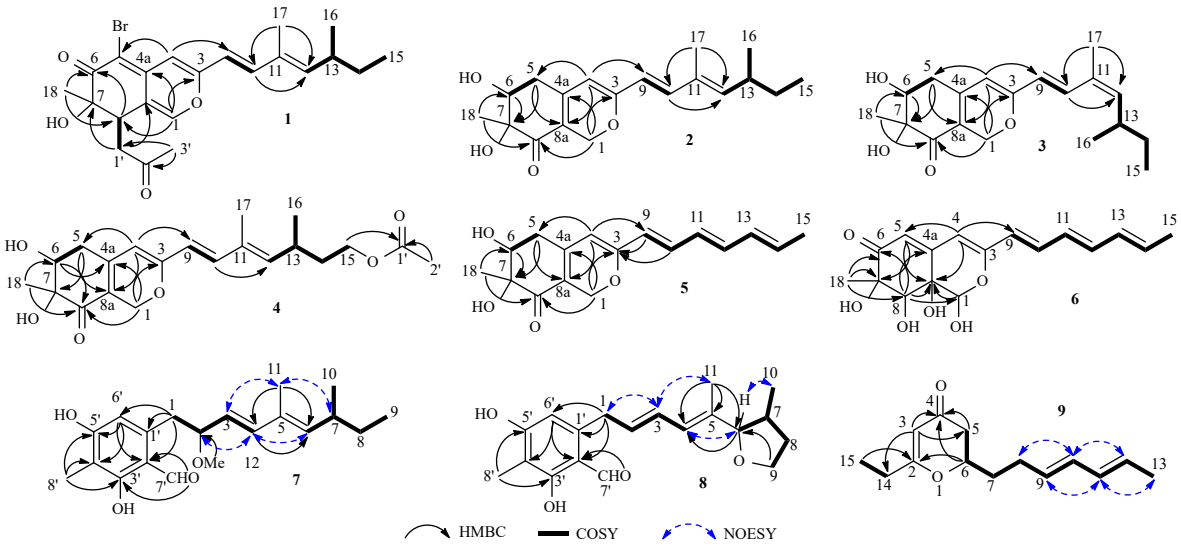

Fig. 2 Key HMBC, ^1H–^1H COSY, and/or NOESY correlations of **1**–**9**.

(Fig. 4) of model-**4** established the (6*R*,7*S*,13*S*)-configuration of **4**.

Isochromophilone K (**5**) was isolated as a yellow oil with a molecular formula of $C_{17}H_{20}O_4$ (8 DOUs), as determined by HR-ESI-MS ion peak. Analysis of the NMR data indicated that **5** was structurally similar to **2**, except for notable differences in the C_7 side chain. Analysis of ^1H–^1H correlation spectroscopy (COSY) correlations of H-9/H-10/H-11/H-12/H-13/H-14/H_3-15 combined with HMBC of H-4/C-9 and H-9, H-10/C-3 confirmed a conjugated triene C_7 side chain attached at C-3 in **5**. The Δ^9, Δ^{11}, and Δ^{13} double bonds in **5** were determined to have *E*-configuration based on the large coupling constant of 15.4 Hz and the NOESY correlation of H_3-15 (δ_H 1.83)/H-13 (δ_H 6.15). The NOESY correl-

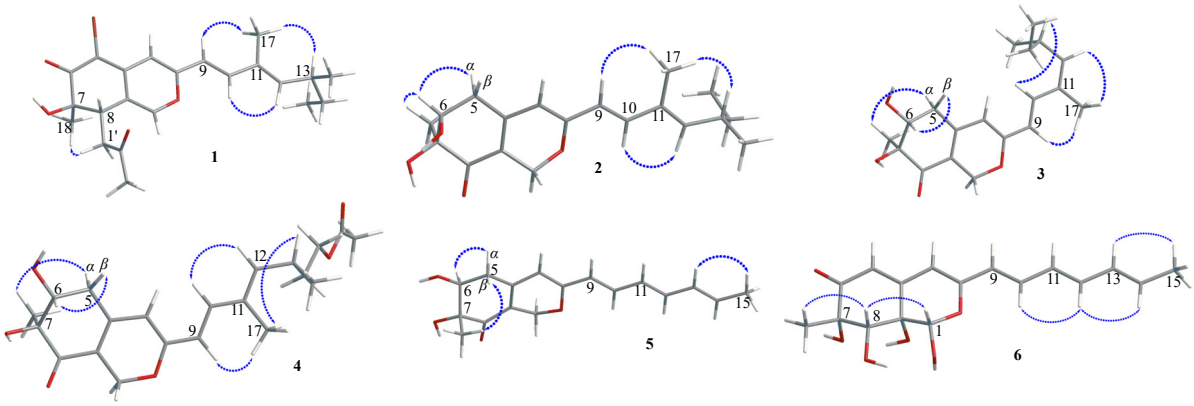

Fig. 3 Key NOESY correlations (blue dashed double arrows) of **1**–**6**.

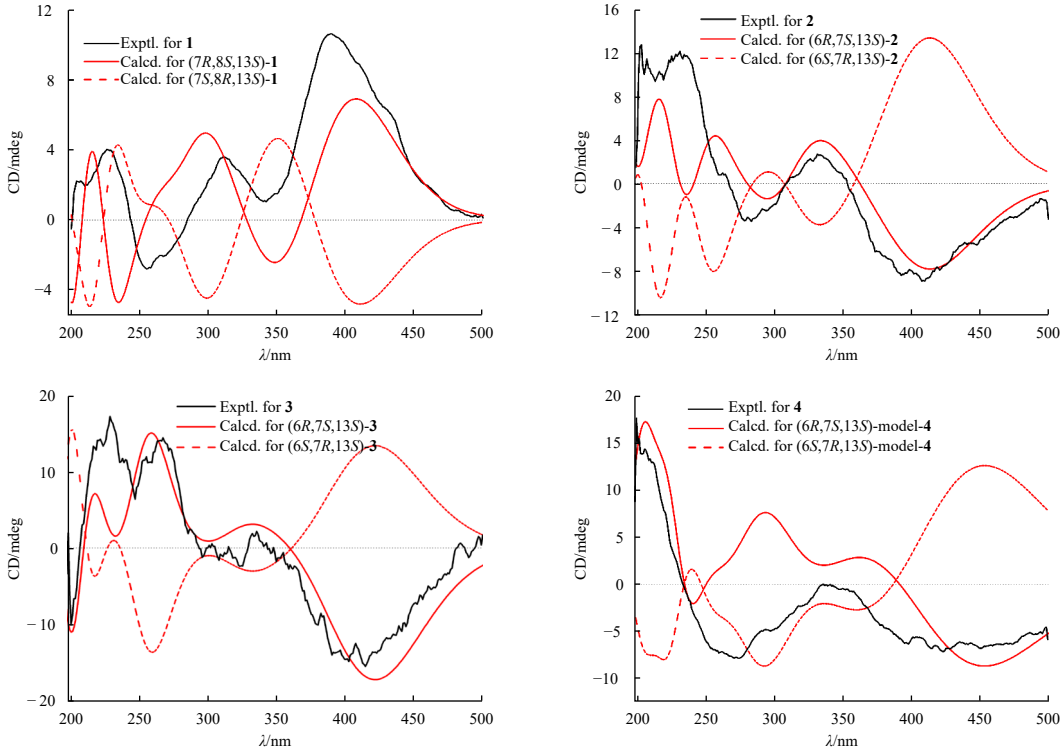

Fig. 4 Experimental and calculated ECD spectra of compounds **1**–**4**.

ations of H-5α (δ_H 2.68)/ H-6 (δ_H 4.03) and H-5β (δ_H 2.49)/H_3-18 (δ_H 1.26) indicated the opposite orientation of H-6 and H_3-18 in the cyclohexanone unit. The (6*S*,7*R*)-configuration of **5** was confirmed through ECD calculations (Fig. S2).

Isochromophilone L (**6**) exhibited the molecular formula $C_{17}H_{20}O_6$ (8 DOUs) as determined by HR-ESI-MS data. The ^{1}H NMR data (Table 1) combined with HSQC experiment of **6** revealed signals of 8 olefinic protons, H-4 (δ_H 5.77, s), H-5 (δ_H 5.71, s), H-9 (δ_H 6.09, d, *J* = 15.4 Hz), H-10 (δ_H 6.98, dd, *J* = 15.4, 11.2 Hz), H-11 (δ_H 6.27, dd, *J* = 15.4, 11.2 Hz), H-12 (δ_H 6.46, dd, *J* = 15.4, 11.2 Hz), H-13 (δ_H 6.19, m), and H-14 (δ_H 5.89, m), a hemiacetal methine H-1 (δ_H 5.40, s) and an oxygenated methine H-8 (δ_H 3.97, s), a singlet methyl H_3-18 (δ_H 1.38) and a doublet one H_3-15 (δ_H 1.81, d, *J* = 7.0 Hz). Additionally, the ^{13}C NMR data of **6** indicated five remaining quaternary carbon resonances, corresponding to one carbonyl (δ_C 199.0), two olefinics (δ_C 153.6 and an oxygenated one 159.6), and two oxygenated tertiary carbons (δ_C 76.4, 71.1). These spectroscopic data suggested **6** as an azaphilone derivative, structurally similar to **5**.

The sequential ^{1}H–^{1}H COSY correlations of H-9/H-10/H-11/H-12/H-13/H-14/H_3-15 and HMBC of H-9/C-3, C-4 in **6** demonstrated that both compounds shared an identical conjugated triene C7 side chain at C-3. In comparison with **5**, the chemical shifts [C-1 (δ_C 97.6), C-5 (δ_C 117.6), C-6 (δ_C 199.0), C-8 (δ_C 74.8), and C-8a (δ_C 71.1)] in **6** indicated a hemiacetal (C-1), an olefinic methine (C-5), a carbonyl carbon (C-6), and three oxygenated carbons (C-7, 8, 8a), further confirmed by HMBC of H-1/C-8a, H-4/C-5, H-5/C-8a, and H-8/C-1, C-8a. The molecular formula supported this structural assignment. Consequently, compound **6** was characterized as a highly oxygenated chrysodin-type azaphilone.

All the Δ^9, Δ^{11}, and Δ^{13} double bonds in **6** were assigned as the shared *E*-configuration through procedures identical to those used for **1**–**5**. The NOESY correlations of H-8/H-1, H_3-18 indicated these protons were co-facial. Subsequently, the relative configuration of **6** was initially assigned as *rel*-(1*S*,7*S*,8*S*) due to the unassigned chiral center of C-8a. Multiple attempts to establish the absolute configurations of **6** using the modified Mosher's method proved unsuccessful, while further investigations were limited by the available quantity. Therefore, four possible stereoi-

somers of **6** underwent ECD calculations. The calculated ECD curves of (1*S*,7*S*,8*S*,8a*S*)-**6** and (1*R*,7*R*,8*R*,8a*S*)-**6** demonstrated a strong correlation with the experimental data (Fig. S2). NMR calculations for these two candidate diastereoisomers of **6** were conducted using the gauge-independent atomic orbital (GIAO) strategy at the mPW1PW91/6-311 + G (d, p) level in the polarizable continuum model (PCM) solvent continuum model with methanol as solvent [25]. The DP4 + probability confirmed the (1*S*,7*S*,8*S*,8a*S*) configurations of **6** with 86% confidence (Fig. S131). Consequently, the absolute configurations of **6** were established as 1*S*, 7*S*, 8*S*, 8a*S*.

Compound **7**, isolated as a colorless oil, exhibited a molecular formula of $C_{20}H_{28}O_4$ (7 DOUs) based on HR-ESI-MS data. The NMR data (Table 3) of **7** closely resembled those of an intermediate, 6-((*S*,3*E*,5*E*)-5,7-dimethyl-2-oxonona-3,5-dien-1-yl)-2,4-dihydroxy-3-methylbenzaldehyde, produced through heterologous expression in *Aspergillus nidulans* [24]. The primary distinction was the presence of a methine ($\delta_{H/C}$ 3.73/83.8) with a methoxy group ($\delta_{H/C}$ 3.19/56.6) in **7** instead of a carbonyl group in the aforementioned intermediate, confirmed by HMBC of H_3-12 (δ_H 3.18)/C-2 (δ_C 83.8). The planar structure of **7** was thus determined and named diaporaldehyde A. The Δ^3 and Δ^5 double bonds maintained the *E*-configuration based on NOESY correlations and coupling constant analysis. Diaporaldehyde A likely serves as a key intermediate in azaphilone biosynthesis [24], suggesting the 7*S* configuration in **7**. ECD calculations (Fig. S2) confirmed the (2*R*,7*S*)-configuration of **7**.

Compound **8** was isolated as a colorless oil with the molecular formula $C_{19}H_{24}O_4$ (8 DOUs) based on HR-ESI-MS data. The ^{1}H NMR data (Table 3) combined with HSQC experiment of **8** revealed signals including an aldehyde group H-7′ (δ_H 10.02, s), 4 aromatic or olefinic protons, H-2 (δ_H 5.85, dt, *J* = 14.7, 7.0 Hz), H-3 (δ_H 6.32, dd, *J* = 14.7, 11.2 Hz), H-4 (δ_H 6.02, d, *J* = 11.2 Hz), and H-6′ (δ_H 6.28, s), a methine H-7 (δ_H 2.05, m) and an oxygenated methine H-6 (δ_H 3.69, d, *J* = 8.4 Hz), 3 methylenes H_2-1 (δ_H 3.67, d, *J* = 7.0 Hz), H_2-8 (δ_H 2.12, m; 1.60, m), and H_2-9 (δ_H 3.89, m; 3.85, m), two singlet methyl, H_3-11 (δ_H 1.68) and H_3-8′ (δ_H 2.00), and a doublet one H_3-10 (δ_H 1.00, d, *J* = 7.0 Hz).

The ^{13}C NMR spectrum of **8** exhibited carbon resonances comprising six aromatic or olefinic carbons (δ_C 136.9, 145.0, 112.8, 110.6; two oxygenated ones, 165.3, 165.1). These spectroscopic characteristics demonstrated significant similarities to those of 6-((*S*,3*E*,5*E*)-5,7-dimethyl-2-oxonona-3,5-dien-1-yl)-2,4-dihydroxy-3-methylbenzaldehyde produced by *Aspergillus nidulans* [24]. The described functionalities accounted for 7 DOUs, with the remaining one DOU necessitating an additional ring in the molecule. The ^{1}H–^{1}H COSY correlations of H-6/H-7/H_2-8/H_2-9 and HMBC of H_2-9/C-6 and H_3-11/C-4, C-5, C-6 enabled the identification of a terminal methyl-substituted tetrahydrofuran located at C-5. Additionally, a conjugated diene moiety linked to C-1′ by a methylene (CH_2-1) in **8** was confirmed through the ^{1}H–^{1}H COSY correlations of H_2-1/H-2/H-3/H-4 and HMBC of H_2-1/C-1′, C-2′, C-6′. Consequently, the planar structure of **8** was determined and designated as diaporaldehyde B. Notably, the tetrahydrofuran ring represents an unusual structural feature in benzaldehyde compounds of this type.

The NOESY correlations of H-3/H_3-11, H_2-1, and H-4/H-6, and the coupling constant of $J_{H\text{-}2/H\text{-}3}$ = 14.7 Hz demonstrated that the Δ^2 and Δ^4 double bonds possessed the *E*-configuration. Furthermore, the NOESY correlation of H-6 (δ_H 3.69)/H_3-10 (δ_H 1.00)

Table 3 ^{1}H (700 MHz) and ^{13}C (175 MHz) NMR data for **7** and **8**.

No.	**7**[a]		**8**[b]	
	δ_C, type	δ_H, (*J* in Hz)	δ_C, type	δ_H, (*J* in Hz)
1	38.4, CH_2	3.09, o; 2.96, o	35.7, CH_2	3.67, d (7.0)
2	83.8, CH	3.73, m	134.0, CH	5.85, dt (14.7, 7.0. 7.0)
3	125.4, CH	5.36, dd (15.4, 8.4)	128.7, CH	6.32, ddd (14.7, 11.2)
4	138.8, CH	6.16 dd (15.4, 5.6)	127.7, CH	6.02, d (11.2)
5	131.5, C		136.9, C	
6	140.8, CH	5.26, d (9.8)	93.0, CH	3.69, d (8.4)
7	34.5, CH	2.38, m	38.7, CH	2.05, m
8	30.4, CH_2	1.36, m; 1.25, m	35.8, CH_2	2.12, m; 1.60, m
9	12.1, CH_3	0.84, t (7.0)	68.7, CH_2	3.89, m; 3.85, m
10	20.7, CH_3	0.96, d (7.0)	16.8, CH_3	1.00, d (7.0)
11	12.9, CH_3	1.72, s	11.8, CH_3	1.68, s
12	56.6, CH_3	3.18, s		
1′	142.3, C		145.0, C	
2′	113.4, C		112.8, C	
3′	164.1, C		165.3, C	
4′	109.5, C		110.6, C	
5′	160.6, C		165.1, C	
6′	110.5, CH	6.24, s	110.4, CH	6.28, s
7′	194.0, CH	10.07, s	194.6, CH	10.02, s
8′	7.1, CH_3	2.09, s	7.2, CH_3	2.00, s

[a]In $CDCl_3$; [b]In CD_3OD; o: overlapped.

indicated that H-6 and Me-10 were positioned on the same face of the tetrahydrofuran ring. Based on the shared biosynthetic origins with co-isolated azaphilones [24], diaporaldehyde B exhibited the 7*S* configuration. Consequently, the absolute configuration of **8** was initially assigned as 6*S*,7*S*, which was subsequently validated by the correspondence between experimental and calculated ECD curves (Fig. S2).

Compound **9** was isolated as a colorless oil with the molecular formula $C_{14}H_{20}O_2$ (5 DOUs), determined from the HR-ESI-MS ion peak of *m/z* 221.1542 $[M + H]^+$ (Calcd. for $C_{14}H_{21}O_2$, 221.1542). Analysis of the 1D (Table 4) and 2D NMR data revealed two distinct parts in **9**. The ^1H–^1H COSY correlations (Fig. 2) of H_2-7/H_2-8/H-9/H-10/H-11/H-12/H_3-13 established a C_7 diene (Δ^9 and Δ^{11}) side chain. The HMBC of H-3/C-2, C-4 (δ_C 193.3), C-5 (δ_C 41.1), H-6/C-2, C-4, and H_2-14 (δ_H 2.27)/C-2 (δ_C 179.0), C-3 ($\delta_{H/C}$ 5.32/103.3), C-15 ($\delta_{H/C}$ 1.13/10.8), and the ^1H–^1H COSY correlations of H_2-14/H_3-15 and H_2-5/H-6, combined with the remaining one DOU, enabled the identification of an *α*, *β*-unsaturated *γ*-pyrone moiety with an ethyl group at C-2. Additionally, the ^1H–^1H COSY correlation of H-6/H_2-7 and HMBC of H-7/C-5, C-6 confirmed the C_7 diene side chain attachment to the *α*, *β*-unsaturated *γ*-pyrone moiety at C-6.

The Δ^9 and Δ^{11} double bonds exhibited the *E*-configuration as evidenced by the NOESY correlations. The 6*S* configuration of **9** was established through comparison of the experimental ECD curve (Fig. S2) of **9** with the calculated spectrum of model-*S*-**9**. Therefore, the structure of **9** was elucidated as (*S*)-6-ethyl-2-((3*E*,5*E*)-hepta-3,5-dien-1-yl)-2,3-dihydro-4*H*-pyran-4-one.

Marine natural products remain relatively unexplored as sources of anti-osteoclastogenic lead compounds [12]. In continuation of our research for novel osteoclast differentiation inhibitors from marine microorganisms [4, 13, 14], the isolated compounds were evaluated for inhibitory effects against RANKL-induced osteoclastogenesis in RAW 264.7 cells using NF-*κ*B luciferase reporter gene as previously described [4]. Notably, compounds **1**, **7**, **10**, and **11** exhibited inhibition of lipopolysaccharide (LPS)-induced NF-*κ*B activation in RAW 264.7 cells at 20 μmol·L^{-1} ($P < 0.001$) (Fig. 5).

Given that NF-*κ*B p65 serves as a crucial factor in RANKL-induced osteoclast differentiation and bone resorption [4], the newly identified potent inhibitor (**1**) was further evaluated for its effects on RANKL-induced osteoclastogenesis in bone marrow macrophages (BMMs) and RAW 264.7 cells using tartrate-resisant acid phosphatase (TRAP) assays, along with cytotoxicity assessment. TRAP activity was measured using *p*-nitrophenyl phosphate, and TRAP-positive multinuclear cells containing more than 5 nuclei for BMMs and more than 3 nuclei for RAW264.7 cells were counted as previously described [4]. Isochromophilone G (**1**) effectively inhibited RANKL-induced osteoclast differentiation in both BMMs (Fig. 6) and RAW264.7 cells (Fig. 7) without demonstrating cytotoxicity, indicating its potential as a novel inhibitor of RANKL-induced osteoclastogenesis. This study presents the first documentation of osteoclast differentiation inhibitory activity for these azaphilones and their related compounds.

3. Experimental

3.1. General experimental procedures

Optical rotations were measured using a Perkin Elmer MPC 500 (Waltham) polarimeter. Ultraviolet (UV) spectra were recorded on a Shimadzu UV-2600 PC spectrometer (Shimadzu). ECD spectra were obtained with a Chirascan circular dichroism spectrometer (Applied Photophysics). Infrared (IR) spectra were recorded on an IR Affinity-1 spectrometer (Shimadzu). NMR spectra were acquired on a Bruker Avance spectrometer (Bruker) operating at 500 MHz and 700 MHz for ^1H NMR, 125 MHz and 175 MHz for ^{13}C NMR, using TMS as an internal standard. HR-ESI-MS spectra were obtained on a Bruker miXis TOF-QII mass spectrometer (Bruker). Thin layer chromatography (TLC) and column chromatography (CC) were performed on plates precoated with silica gel GF_{254} (10–40 μm) and over silica gel (200–300 mesh) (Qingdao Marine Chemical Factory), and Sephadex LH-20 (Amersham Biosciences), respectively. Spots were visualized on TLC (Qingdao Marine Chemical Factory) under 254 nm UV light. All solvents used were of analytical grade (Tianjin Fuyu Chemical and Industry Factory). Semi-preparative HPLC was conducted using an octadecylsilane (ODS) column (YMC-pack ODS-A, YMC Co. Ltd., 10 mm × 250 mm, 5 μm, 2.5 mL·min^{-1}).

3.2. Fungal material

The fungi *Diaporthe* sp. SCSIO 41011 was isolated from a mangrove plant, *Rhizophora stylosa*, as previously described [20]. A voucher specimen has been deposited in the Guangdong Microbial Culture Collection Center (GDMCC No. 60671).

3.3. Fermentation and extraction

The strain *Diaporthe* sp. SCSIO 41011 was cultivated on MB-agar plates at 25 °C for 7 d. The seed medium (malt extract 15 g and NaBr 15 g in 1.0 L tap distilled H_2O, pH 7.4–7.8) was inoculated with strain SCSIO 41011 and incubated at 25 °C for 3 d on a rotating shaker (180 r·min^{-1}). Subsequently, a large-scale fermentation of fungal isolate SCSIO 41011 was conducted for 30 d at room temperature in 1 L × 60 conical flasks containing solid rice medium (each flask contained 150 g wheat, 2.7 g NaBr, 1.8 g peptone, and 180 mL H_2O). The fermented cultures were extracted with EtOAc three times, and the solvent was concentrated under vacuum to yield a crude extract (50 g).

3.4. Isolation and purification

The EtOAc extract underwent fractionation through silica gel medium pressure liquid chromatography using a gradient solvent

Table 4 ^1H (700 MHz) and ^{13}C (175 MHz) NMR data of **9** ($CDCl_3$).

No.	δ_C, type	δ_H, (*J* in Hz)	No.	δ_C, type	δ_H, (*J* in Hz)
2	179.0, C		9	129.8, CH	5.52, m
3	103.3, CH	5.32, s	10	131.4, CH	6.02, overlapped
4	193.3, C		11	131.7, CH	6.00, overlapped
5	41.1, CH_2	2.41, dd (16.8, 13.3) 2.37, dd (16.8, 4.2)	12	128.0, CH	5.61, overlapped
6	78.5, CH	4.35, m	13	18.2, CH_3	1.74, d (6.3)
7	34.2, CH_2	1.92, m; 1.72, m	14	28.1, CH_2	2.27, m
8	28.0, CH_2	2.23, m	15	10.8, CH_3	1.13, t (7.0)

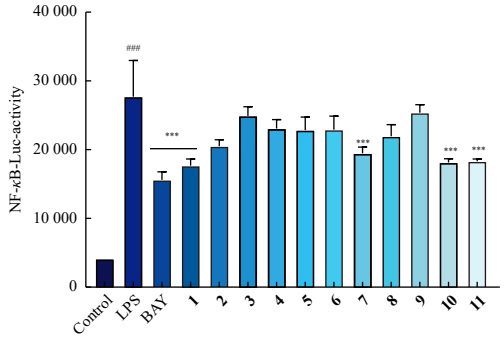

Fig. 5 The inhibitory effects of compounds **1**–**11** on LPS-induced NF-κB activation in RAW264.7 cells at 20 μmol·L^{-1}. Data are presented as the mean ± SD (n = 3). $^{###}P$ < 0.001 *vs* control group (untreated); $^{***}P$ < 0.001 *vs* LPS-induced group. BAY (BAY11-7082, positive control).

system of petroleum ether/CH_2Cl_2 (0–100%), yielding 7 fractions based on TLC analysis. Fraction 2 was further separated into 7 subfractions (Frs. 2-1–2-7) using ODS silica gel chromatography with MeOH/H_2O (10%–100%) as eluent. Fr. 2-5 was subsequently purified by semipreparative HPLC (82% MeOH/H_2O, 2.5 mL·min^{-1}) to obtain **9** (3 mg, t_R 16 min) and **7** (1.5 mg, t_R 24 min). Compound **1** (5 mg, t_R 34 min) was isolated from Fr. 4 through ODS silica gel chromatography with MeOH/H_2O (10%–100%) followed by semipreparative HPLC (79% MeOH/H_2O + 0.02% trifluoroacetic acid (TFA), 2 mL·min^{-1}). Fraction 5 was separated into 10 subfractions (Frs. 5-1–5-10) using ODS silica gel chromatography with MeOH/H_2O (10%–100%). Fr. 5-5 was purified by semipreparative HPLC (70% MeOH/H_2O, 2 mL·min^{-1}) to yield **10** (8 mg, t_R 15 min). Compounds **2** (2 mg, t_R 18 min) and **8** (4 mg, t_R 22 min) were isolated from Fr. 5-8 using semipreparative HPLC (84% MeOH/H_2O, 2 mL·min^{-1}). Fr. 5-10 was purified by semipreparative HPLC (85% MeOH/H_2O + 0.02%TFA, 2 mL·min^{-1}) to obtain **11** (3 mg, t_R 20 min). Fraction 6 was separated into 9 subfractions (Frs. 6-1–6-9) using ODS silica gel chromatography with MeOH/H_2O (10%–100%). Compound **3** (1 mg, t_R 22 min) was isolated from Fr. 6-6 through semipreparative HPLC (79% MeOH/H_2O, 2 mL·min^{-1}). Fr. 6-7 was purified by semipreparative HPLC (68% MeOH/H_2O, 2 mL·min^{-1}) to yield **6** (3 mg, t_R 30 min) and **5** (1 mg, t_R 33 min). Compound **4** (4 mg, t_R 30 min) was obtained from Fr. 6-8 through semipreparative HPLC (68% MeOH/H_2O, 2 mL·min^{-1}).

Isochromophilone G (**1**): yellow solid; $[\alpha]_D^{25}$ +154 (*c* 0.09, MeOH); UV (MeOH) λ_{max} (log ε) 389 (3.33), 250 (3.29), 200 (3.38) nm; ECD (0.25 mg·mL^{-1}, MeOH) λ_{max} ($\Delta\varepsilon$) 389 (+5.59), 340

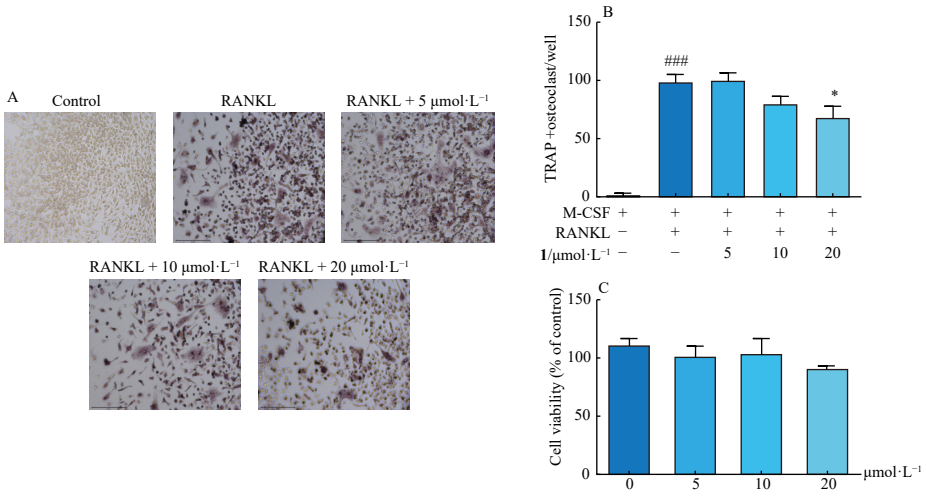

Fig. 6 Inhibitory effects of **1** on RANKL-induced osteoclastogenesis in BMMs. A) Representative images showing that RANKL-induced osteoclast differentiation was inhibited by compound **1** in BMMs. (magnification = 100 × ; scale bar = 500 μm). B) TRAP-positive multinucleated cells (nuclei ≥ 5) in the presence of **1** were counted. C) Cell viability of **1** against BMMs for 72 h was measured by MTT assay. Data are presented as the mean ± SD (n = 3). $^{###}P$ < 0.001 *vs* control group; $^{*}P$ < 0.05 *vs* RANKL group.

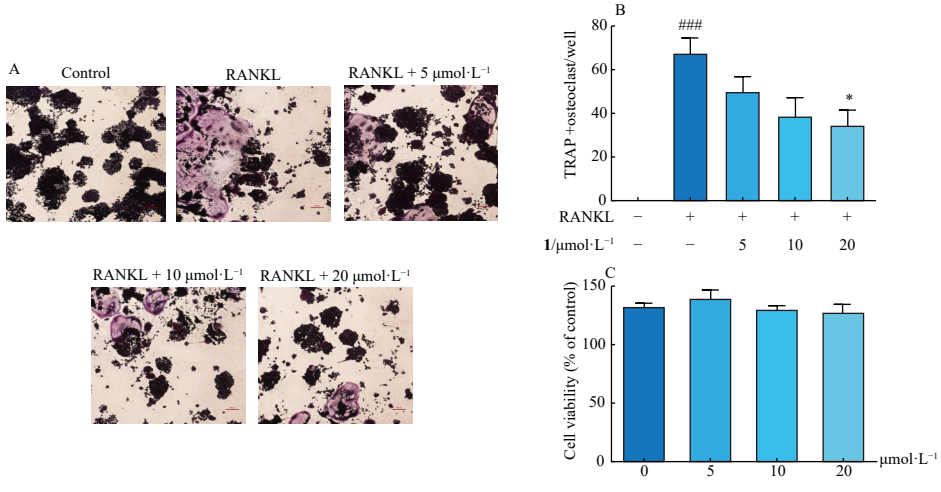

Fig. 7 Inhibitory effects of **1** on RANKL-induced osteoclastogenesis in RAW264.7 cells. (A) Representative images showing that RANKL-induced osteoclast differentiation was inhibited by compound **1** in RAW264.7 cells. (magnification = 100 × ; scale bar = 500 μm). (B) TRAP-positive multinucleated cells (nuclei ≥ 3) in the presence of **1** were counted. (C) Cell viability of **1** against RAW264.7 cells for 72 h were measured by MTT assay. Data are presented as the mean ± SD (n = 3). $^{###}P$ < 0.001 *vs* control group; $^{*}P$ < 0.05 *vs* RANKL group.

(+0.54), 311 (+1.90), 255 (−1.49), 226 (+2.11) nm; IR (film) ν_{max} 3429, 2927, 1716, 1662, 1514, 1367, 1165 cm^{-1}; ^1H and ^{13}C NMR data, Tables 1 and 2; HR-ESI-MS *m/z* 435.1177 $[M + H]^+$ (Calcd. for $C_{22}H_{28}BrO_4$, 435.1171).

Isochromophilone H (**2**): yellow solid; $[\alpha]_D^{25}$ −4.4 (*c* 0.05, MeOH); UV (MeOH) λ_{max} (log *ε*) 388 (2.89), 231 (3.11), 200 (3.21) nm; ECD (0.3 mg·mL^{-1}, MeOH) λ_{max} (Δ*ε*) 410 (−0.44), 332 (+0.29), 284 (−0.10), 235 (+0.86) nm; IR (film) ν_{max} 3398, 2926, 1674, 1635, 1521, 1456, 1404, 1373, 1190 cm^{-1}; ^1H and ^{13}C NMR data, Tables 1 and 2; HR-ESI-MS *m/z* 319.1912 $[M + H]^+$ (Calcd. for $C_{19}H_{27}O_4$, 319.1909), 341.1733 $[M + Na]^+$ (Calcd. for $C_{19}H_{26}NaO_4$, 341.1729).

Isochromophilone I (**3**): yellow solid; $[\alpha]_D^{25}$ −15.9 (*c* 0.12, MeOH); UV (MeOH) λ_{max} (log *ε*) 403 (3.67), 272 (3.67), 262 (3.69), 231 (3.90), 204 (3.93) nm; ECD (0.15 mg·mL^{-1}, MeOH) λ_{max} (Δ*ε*) 415 (−0.89), 344 (+0.04), 270 (+0.68), 225 (+0.67), 204 (−0.60) nm; IR (film) ν_{max} 3446, 2931, 1749, 1716, 1697, 1653, 1558, 1541, 1506, 1456, 1029 cm^{-1}; ^1H and ^{13}C NMR data, Tables 1 and 2; HR-ESI-MS *m/z* 319.1903 $[M + H]^+$ (Calcd. for $C_{19}H_{27}O_4$, 319.1909), 341.1724 $[M + Na]^+$ (Calcd. for $C_{19}H_{26}NaO_4$, 341.1729).

Isochromophilone J (**4**): yellow solid; $[\alpha]_D^{25}$ +17 (*c* 0.07, MeOH); UV (MeOH) λ_{max} (log *ε*) 401 (3.05), 263 (3.06), 200 (3.26) nm; ECD (0.25 mg·mL^{-1}, MeOH) λ_{max} (Δ*ε*) 424 (−0.20), 342 (+0.81), 272 (−0.30), 313 (+2.86) nm; IR (film) ν_{max} 3408, 2929, 1734, 1635, 1519, 1406, 1373, 1244, 1033 cm^{-1}; ^1H and ^{13}C NMR data, Tables 1 and 2; HR-ESI-MS *m/z* 377.1962 $[M + H]^+$ (Calcd. for $C_{21}H_{29}O_6$, 377.1964).

Isochromophilone K (**5**): yellow solid; $[\alpha]_D^{25}$ +21.7 (*c* 0.07, MeOH); UV (MeOH) λ_{max} (log *ε*) 388 (2.84), 227 (3.07), 200 (3.20) nm; ECD (0.35 mg·mL^{-1}, MeOH) λ_{max} (Δ*ε*) 401 (+0.78), 334 (−0.19), 252 (+0.71), 219 (−1.05) nm; IR (film) ν_{max} 3396, 2929, 1716, 1683, 1653, 1541, 1506, 1456, 1417, 1192, 1070 cm^{-1}; ^1H and ^{13}C NMR data, Tables 1 and 2; HR-ESI-MS *m/z* 289.1444 $[M + H]^+$ (Calcd. for $C_{17}H_{21}O_4$, 289.1440).

Isochromophilone L (**6**): yellow solid; $[\alpha]_D^{25}$ +24.3 (*c* 0.07, MeOH); UV (MeOH) λ_{max} (log *ε*) 380 (3.25), 268 (2.82), 200 (3.05) nm; ECD (0.25 mg·mL^{-1}, MeOH) λ_{max} (Δ*ε*) 343 (+0.68), 302 (+0.06), 287 (+0.43), 248 (−0.05), 203 (−1.50) nm; IR (film) ν_{max} 3379, 2929, 1653, 1575, 1417, 1396, 1118, 1064 cm^{-1}; ^1H and ^{13}C NMR data, Tables 1 and 2; HR-ESI-MS *m/z* 321.1328 $[M + H]^+$ (Calcd. for $C_{17}H_{21}O_6$, 321.1338).

Diaporaldehyde A (**7**): colorless oil; $[\alpha]_D^{25}$ +18 (*c* 0.10, MeOH); UV (MeOH) λ_{max} (log *ε*) 231 (3.92), 294 (3.47) nm; ECD (0.20 mg·mL^{-1}, MeOH) λ_{max} (Δ*ε*) 202 (+1.28), 234 (0.99) nm; IR (film) ν_{max} 3292, 2958, 1683, 1635, 1558, 1506, 1489, 1456, 1417, 1251, 1122 cm^{-1}; ^1H and ^{13}C NMR data, Table 3; HR-ESI-MS *m/z* 355.1896 $[M + Na]^+$ (Calcd. for $C_{20}H_{28}NaO_4$, 355.1885).

Diaporaldehyde B (**8**): colorless oil; $[\alpha]_D^{25}$ +24 (*c* 0.10, MeOH); UV (MeOH) λ_{max} (log *ε*) 242 (3.94), 297 (3.64) nm; ECD (0.20 mg·mL^{-1}, MeOH) λ_{max} (Δ*ε*) 237 (+3.00) nm; IR (film) ν_{max} 3259, 2960, 2872, 1614, 1456, 1307, 1249, 1124, 1026 cm^{-1}; ^1H and ^{13}C NMR data, Table 3; HR-ESI-MS *m/z* 317.1750 $[M + H]^+$ (Calcd. for $C_{19}H_{25}O_4$, 317.1753), 339.1571 $[M + Na]^+$ (Calcd. for $C_{19}H_{24}NaO_4$, 339.1572).

(*S*)-6-ethyl-2-((3*E*,5*E*)-hepta-3,5-dien-1-yl)-2,3-dihydro-4*H*-pyran-4-one (**9**): colorless oil; $[\alpha]_D^{25}$ −38.5 (*c* 0.10, MeOH); UV (MeOH) λ_{max} (log *ε*) 227 (3.74), 264 (3.48) nm; ECD (0.20 mg·mL^{-1}, MeOH) λ_{max} (Δ*ε*) 232 (−1.85), 250 (−0.27), 267 (−0.56), 288 (−0.07), 313 (−0.58) nm; IR (film) ν_{max} 3416, 2935, 2877, 1666, 1602, 1406, 1240, 1205, 1138, 1020 cm^{-1}; ^1H and ^{13}C NMR data, Table 4; HR-ESI-MS *m/z* 221.1542 $[M + H]^+$ (Calcd. for $C_{14}H_{21}O_2$, 221.1542), 243.1360 $[M + Na]^+$ (Calcd. for $C_{14}H_{20}NaO_2$, 243.1361).

3.5. ECD calculations

Conformational searches were conducted using the Spartan'14 software (Wavefunction Inc., Irvine, CA, USA) employing the Merck Molecular Force Field (MMFF) method as previously described [20]. The MMFF minima were subsequently re-optimized through DFT calculations at the B3LYP/6-31 + g (d, p) level utilizing the PCM *via* Gaussian 16 software. The theoretical ECD calculations were performed in MeOH by TDDFT at the B3LYP/6-311 + G (d, p) level for the low-energy conformers using 50 excited states. ECD spectra were generated using the program SpecDis 1.7 (University of Würzburg) and Prism 5.0 (GraphPad Software Inc.) with a half-bandwidth of 0.2–0.4 eV (Table S1), based on the Boltzmann-calculated contribution of each conformer after UV correction. Additionally, the stable conformers of the two diastereomers of 6 with Boltzmann populations exceeding 1% were selected for NMR chemical shift calculations using the gauge-including atomic orbital (GIAO) method at the PCM//mPW1PW91/6-311 + G (d, p) level of theory for DP4 + calculations as described previously [25]. The DP4 + calculations were executed using the Excel spreadsheet available at sarotti-NMR.weebly.com.

3.6. Anti-osteoclastogenic bioassay

The isolated compounds (**1**–**11**) were initially evaluated for their inhibitory activities of LPS-induced NF-*κ*B activation in RAW264.7 cells by NF-*κ*B luciferase reporter gene assay as previously described [4, 13]. RAW264.7 cells stably transfected with an NF-*κ*B luciferase reporter gene were pretreated with these compounds (20 μmol·L^{-1}) and BAY11-7082 (a typical NF-*κ*B inhibitor as positive control, 5 μmol·L^{-1}, Sigma-Aldrich) in 96-well plates for 30 min, followed by 5 μg·mL^{-1} LPS stimulation for 8 h. For the anti-osteoclastogenesis assay, compound **1** (5, 10, and 20 μmol·L^{-1}) was added to BMMs with both M-CSF (50 ng·mL^{-1}) and RANKL (100 ng·mL^{-1}) stimulation for 3 d. Subsequently, compound **1** (5, 10, and 20 μmol·L^{-1}) was added to RAW264.7 cells with RANKL (100 ng·mL^{-1}) stimulation for 5 days. The cells were then fixed and stained for TRAP activity, and the images were captured by an inverted microscope (Nikon, Japan). Additionally, the MTT assay kit was utilized to evaluate the cytotoxic effects of **1** (5, 15, 20 μmol·L^{-1}) on BMMs (1 × 10^5 cells/mL) for 72 h. Data were expressed as the mean ± SD and analyzed using GraphPad Prism 7.0 software (San Diego, CA, USA). Statistical differences among groups were determined using one-way analysis of variance (ANOVA) with a Bonferroni *post-hoc* test. A level of $P < 0.05$ was considered statistically significant.

4. Conclusion

This study identified six new azaphilones and three new biosynthetically related siblings from *Diaporthe* sp. SCSIO 41011 through the OSMAC approach. Their structures and absolute configurations were established through comprehensive NMR, MS spectroscopic analyses, and ECD calculations. Structurally, three highly oxygenated azaphilones contain linear polyenoid moieties and/or an acetyl group attached to the terminal chain, representing uncommon features in the azaphilone family. The structural diversity and complexity of azaphilones primarily arise from extensive modifications of the pyranoquinone bicyclic core and polyketide side chain length. Furthermore, several compounds demonstrated inhibition of LPS-induced NF-*κ*B in RAW 264.7 macrophages at 20 μmol·L^{-1}. Significantly, the novel and most potent compound (**1**) inhibited RANKL-induced osteoclast differentiation without apparent cytotoxicity in BMMs, indicating its potential as a promising lead compound for osteolytic disease treatment. These findings expand the chemical and bioactive diversity of azaphilones and establish a foundation for the further development of azaphilones as potential anti-osteoporosis therapeutic agents.

Funding

This work was supported by the National Natural Science Foundation of China (No. 82260692), Guangxi Natural Science Foundation (No. 2024GXNSFFA010004), Bagui Youth Talent Development Program, High-Level Talent Training Project Foundation of Guangxi University of Chinese Medicine (Nos. 202407 and 2022C038), and the Innovation Project of Guangxi Graduate Education (No. YCSW2025457).

Supplementary data

Supplementary data for this paper is available upon email request to the corresponding authors.

Declaration of competing interest

The authors declare no competing financial interest.

References

1 Eastell R, O'Neill TW, Hofbauer LC, et al. Postmenopausal osteoporosis. *Nat Rev Dis Primers*. 2016;2(1):16069. https://doi.org/10.1038/nrdp.2016.69.
2 Rachner TD, Khosla S, Hofbauer LC. Osteoporosis: now and the future. *Lancet*. 2011;377(9773):1276-1287. https://doi.org/10.1016/S0140-6736(10)62349-5.
3 Zhao XL, Feng YX, Peng Y. Prevention and treatment of osteoporosis with Chinese Herbal Medicines. *Chin Herb Med*. 2012;(4):265-270. https://doi.org/10.3969/j.issn.1674-6348.2012.04.001
4 Tan YH, Deng WD, Zhang YY, et al. A marine fungus-derived nitrobenzoyl sesquiterpenoid suppresses receptor activator of NF-κB ligand-induced osteoclastogenesis and inflammatory bone destruction. *Brit J Pharmacol*. 2020;177(18):4242-4260. https://doi.org/10.1111/bph.15179.
5 McDonald MM, Khoo WH, Ng PY, et al. Osteoclasts recycle *via* osteomorphs during RANKL-stimulated bone resorption. *Cell*. 2021;184(5):1330-1347. https://doi.org/10.1016/j.cell.2021.03.010.
6 Huang DE, Zhao C, Li RY, et al. Identification of a binding site on soluble RANKL that can be targeted to inhibit soluble RANK-RANKL interactions and treat osteoporosis. *Nat Commun*. 2022;13(1):5338. https://doi.org/10.1038/s41467-022-33006-4.
7 Boyle WJ, Simonet WS, Lacey DL. Osteoclast differentiation and activation. *Nature*. 2003;423(6937):337-342. https://doi.org/10.1038/nature01658.
8 Wang XY, Yamauchi K, Mitsunaga T. A review on osteoclast diseases and osteoclastogenesis inhibitors recently developed from natural resources. *Fitoterapia*. 2020;142:104482. https://doi.org/10.1016/j.fitote.2020.104482.
9 Carroll AR, Copp BR, Davis RA, et al. Marine natural products. *Nat Prod Rep*. 2024;41(2):162-207. https://doi.org/10.1039/D3NP00061C.
10 Chen SH, Cai RL, Liu ZM, et al. Secondary metabolites from mangrove-associated fungi: source, chemistry and bioactivities. *Nat Prod Rep*. 2022;39:560-595. https://doi.org/10.1039/D1NP00041A.
11 Li KL, Chen SQ, Pang XY, et al. Natural products from mangrove sediments-derived microbes: structural diversity, bioactivities, biosynthesis, and total synthesis. *Eur J Med Chem*. 2022;230:114117. https://doi.org/10.1016/j.ejmech.2022.114117.
12 El-Desoky AHH, Tsukamoto S. Marine natural products that inhibit osteoclastogenesis and promote osteoblast differentiation. *J Nat Med*. 2022;76(3):575-583. https://doi.org/10.1007/s11418-022-01622-5.
13 Zhang YT, Li ZC, Huang BY, et al. Anti-osteoclastogenic and antibacterial effects of chlorinated polyketides from the Beibu Gulf coral-derived fungus *Aspergillus unguis* GXIMD 02505. *Mar Drugs*. 2022;20(3):178. https://doi.org/10.3390/md20030178.
14 Lu HM, Tan YH, Zhang YT, et al. Osteoclastogenesis inhibitory phenolic derivatives produced by the Beibu Gulf coral-associated fungus *Acremonium sclerotigenum* GXIMD 02501. *Fitoterapia*. 2022159:105201. https://doi.org/10.1016/j.fitote.2022.105201.
15 Cai J, Gao L, Wang Y, et al. Discovery of a novel anti-osteoporotic agent from marine fungus-derived structurally diverse sirenins. *Eur J Med Chem*. 2024;265:116068. https://doi.org/10.1016/j.ejmech.2023.116068.
16 Wang WH, Lee J, Kim KJ, et al. Austalides, osteoclast differentiation inhibitors from a marine-derived strain of the fungus *Penicillium rudallense*. *J Nat Prod*. 2019;82(11):3083-3088. https://doi.org/10.1021/acs.jnatprod.9b00690.
17 Gao JM, Yang SX, Qin JC. Azaphilones: chemistry and biology. *Chem Rev*. 2013;113(7):4755-4811. https://doi.org/10.1021/cr300402y.
18 Pavesi C, Flon V, Mann S, et al. Biosynthesis of azaphilones: a review. *Nat Prod Rep*. 2021;38(6):1058-1071. https://doi.org/10.1039/D0NP00080A.
19 Chen CM, Tao HM, Chen WH, et al. Recent advances in the chemistry and biology of azaphilones. *RSC Adv*. 2020;10(17):10197-10220. https://doi.org/10.1039/d0ra00894j.
20 Luo XW, Lin XP, Tao HM, et al. Isochromophilones A–F, cytotoxic chloroazaphilones from the marine mangrove endophytic fungus *Diaporthe* sp. SCSIO 41011. *J Nat Prod*. 2018;81(4):934-941. https://doi.org/10.1021/acs.jnatprod.7b01053.
21 Zang Y, Gong YH, Chen X, et al. Piperazine-2,5-dione derivatives and an α-pyrone polyketide from *Penicillium griseofulvum* and their immunosuppression activity. *Phytochemistry*. 2021;186:112708. https://doi.org/10.1016/j.phytochem.2021.112708.
22 Chen YM, Wang SX, Shen YC. Chemical constituents from *Ainsliaea glabra*. *Guihaia*. 2014;34(03):402-407. https://doi.org/10.3969/j.issn.1000-3142.
23 Jiang HM, Cai RL, Zang ZM, et al. Azaphilone derivatives with anti-inflammatory activity from the mangrove endophytic fungus *Penicillium sclerotiorum* ZJHJJ-18. *Bioorg Chem*. 2022;122:105721. https://doi.org/10.1016/j.bioorg.2022.105721.
24 Chiang YM, Oakley CE, Ahuja M, et al. An efficient system for heterologous expression of secondary metabolite genes in *Aspergillus nidulans*. *J Am Chem Soc*. 2013;135(20):7720-7731. https://doi.org/10.1021/ja401945a.
25 Luo XW, Chen CM, Tao HM, et al. Structurally diverse diketopiperazine alkaloids from the marine-derived fungus *Aspergillus versicolor* SCSIO 41016. *Org Chem Front*. 2019;6(6):736-740. https://doi.org/10.1039/C8QO01147H.